

# Heating Dynamics of Correlated Fermions under Dephasing

Antonio Picano,<sup>1</sup> Matthieu Vanhoecke,<sup>1</sup> and Marco Schirò<sup>1</sup>

<sup>1</sup>*JEIP, UAR 3573 CNRS, Collège de France, PSL Research University,  
11, place Marcelin Berthelot, 75231 Paris Cedex 05, France*

(Dated: July 30, 2025)

We study the dissipative dynamics of correlated fermions evolving in presence of a local dephasing bath. To this extent we consider the infinite coordination limit of the corresponding Lindblad master equation, provided by Dynamical Mean-Field Theory for open quantum systems. We solve the resulting quantum impurity problem, describing an Anderson impurity coupled to a local dephasing, using weak-coupling perturbation theory in interaction and dephasing. We show that the dissipative dynamics describes heating towards infinite temperature, with a relaxation rate that depends strongly on interaction. The resulting steady-state spectral functions are however non-trivial and show an interplay between coherent quasiparticle peak and local dephasing. We then discuss how thermalization towards infinite temperature emerges within DMFT, by solving the impurity problem throughout its self-consistency. We show that thermalization under open quantum system dynamics is qualitatively different from the closed system case. In particular, the thermalization front found in the unitary is strongly modified, a signature of the irreversibility of the open system dynamics.

## I. INTRODUCTION

Open quantum many-body systems where coherent evolution competes with dissipative dynamics due to coupling to external environments are currently attracting widespread interest [1, 2]. A popular framework to describe dissipation which is relevant for several experimental platforms across atomic physics, solid state and quantum optics, is the Lindblad master equation which describes Markovian open quantum system dynamics [3].

Among the different dissipative mechanisms, dephasing due to energy exchange with a hot bath has been studied extensively [4–16]. Several works have focused on the dissipation induced heating and the effect of many-body interactions on the heating dynamics [17–20]. In particular, for bosonic systems, this has been triggered by pioneering theoretical and experimental works [21–25]. The heating dynamics of many-body interacting fermionic systems has been less explored, even though few results are available systems [26–30]. This topic is particularly relevant to both quantum simulation experiments [31] and solid state physics. Indeed, recent progress in quantum simulations of fermionic gases in optical lattices have achieved record breaking cold temperatures and started to reveal intriguing features of strong correlation physics [32, 33]. An important issue is to understand the mechanisms for heating production. In solid-state context dephasing can be seen to arise from the coupling to a hot phonon bath [34].

At the more fundamental level the question of how quantum many-body system heat up is relevant for many different nonequilibrium problems. The case of dephasing is particularly appealing in this respect since one expects thermalization towards a featureless infinite temperature state. How precisely this thermalization arises in a quantum many-body system and the role of the self-consistent environment made by the rest of the system is unclear and largely unexplored. Furthermore, the connection be-

tween unitary evolution where memory of the initial condition is preserved indefinitely, and dissipative dynamics which admits a well defined steady state is worth to be explored, particularly in a regime where dissipation is parametrically weak with respect to coherent energy scales.

In this work we tackle these questions by studying the dissipative dynamics of correlated fermions, described by a Fermi-Hubbard model, evolving in presence of a local dephasing bath. To this extent we consider the infinite coordination limit of the corresponding Lindblad master equation, provided by Dynamical Mean-Field Theory (DMFT) for open quantum systems [35–37]. We solve the resulting quantum impurity problem, describing an Anderson impurity coupled to a local dephasing [38, 39], using weak-coupling perturbation theory in interaction and dephasing. We show that the dissipative dynamics describes heating towards infinite temperature, with a relaxation rate that depends strongly on interaction. The resulting steady-state spectral functions are however non-trivial and show an interplay between coherent quasiparticle peak and local dephasing. We then discuss how thermalization towards infinite temperature emerges within DMFT, by solving the impurity problem throughout its self-consistency. We show that thermalization under open quantum system dynamics is qualitatively different from the closed system case. While the latter is characterized by a ballistic thermalisation front that signals the emergence of a self-consistent bath [40], the irreversible dissipative dynamics does not retain memory of initial condition and so lack any sharp front.

The paper is structured as follows. In Sec. II we introduce the Hubbard model and the dissipative dynamics with dephasing that will be the focus of this work. In Sec. III we present a self-contained introduction to DMFT for open quantum many-body systems and describe the impurity solver used in our work to solve DMFT equations. Sec. IV contains our results concern-

ing the dynamics after a quench of the dephasing, while in Sec. V we discuss the dynamics after photoexcitation and a simultaneous quench of the dephasing. In Sec. VI we discuss and interpret the emergence of infinite temperature thermalization in DMFT. Finally, Sec. VII is devoted to discussions and conclusions. Several technical Appendix complete this work with further details and results.

## II. MODEL AND DYNAMICS

We consider a system of interacting fermionic particles on a lattice with coordination number  $z$ , coupled to a dissipative bath (see sketch in Fig. 1). The many-body density matrix of the system  $\rho_t$  evolves according to a Lindblad master equation [3]

$$\partial_t \rho_t = -i[H, \rho_t] + \sum_{i,\sigma} L_{i\sigma} \rho_t L_{i\sigma}^\dagger - \frac{1}{2} \{L_{i\sigma}^\dagger L_{i\sigma}, \rho_t\} \quad (1)$$

with a set of jump operators  $L_{i\sigma}$ , which we assume to be local at each site, accounting for dissipative processes. The index  $i$  corresponds to the site index, while  $\sigma$  represents the spin. The coherent evolution is governed by the Hubbard Hamiltonian which reads,

$$H = -\frac{t_h}{\sqrt{z}} \sum_{\langle i,j \rangle, \sigma} c_{i\sigma}^\dagger c_{j\sigma} + U \sum_i \left( n_{i\uparrow} - \frac{1}{2} \right) \left( n_{i\downarrow} - \frac{1}{2} \right) \quad (2)$$

where the hopping  $t_h$  is restricted to next-neighboring sites,  $n_{i\sigma} = c_{i\sigma}^\dagger c_{i\sigma}$  is the spin-density operator for spin  $\sigma$  on site  $i$ , and  $U$  is the Coulomb energy. In the following, we consider a Bethe lattice, with hopping  $t_h = 1$  setting the unit of energy and semi-elliptic density of states  $D(\epsilon) = \sqrt{4 - \epsilon^2}/(2\pi)$ . For what concerns the local dissipative dynamics, we consider the case of dephasing, corresponding to jump operators of the form

$$L_{i\sigma} = \sqrt{\gamma} n_{i\sigma} \quad (3)$$

where  $\gamma$  is the dephasing rate associated to the spin  $\sigma$ . This type of dissipation describes energy exchange with a collection of independent baths at infinite temperature. Indeed one can show that the total energy  $E(t) = \text{Tr}(\rho_t H)$  is not conserved under the Lindblad dynamics with Eq. (3). On the contrary, the total number of particle is conserved both under the unitary part of the dynamics as well as by the dissipation. Since the jump operators are Hermitian one can easily show that the trivial density matrix  $\rho_\infty = 1$ , corresponding to a featureless infinite temperature state, is a steady state of the Lindblad dynamics for any finite system size.

In the following we will discuss the dynamics of the system after two types of nonequilibrium protocols (see sketch in Fig. 1): (a) A sudden switching-on of the dephasing starting from an equilibrium configuration; (b)

the dynamics after a photoexcitation and simultaneous quench of the dissipation, see details below. In both cases, we discuss the approach to the steady state as well as the spectral functions in the steady-state. Before presenting our results we briefly discuss the method used to solve our model.

## III. OUT-OF-EQUILIBRIUM DMFT FOR MARKOVIAN FERMIONS

To investigate the out-of-equilibrium dynamics of the dissipative Hubbard model introduced in Sec. II, we employ an extension of dynamical mean-field theory (DMFT) to Markovian open quantum systems [37]. This approach allows us to nonperturbatively treat local quantum correlations while capturing the effects of both coherent evolution and Markovian dissipation. In particular, we consider the infinite coordination number limit  $z \rightarrow \infty$  of the Bethe lattice, where DMFT becomes exact, and the lattice problem can be mapped onto a quantum impurity problem subject to a self-consistently determined bath.

The starting point for writing DMFT for Markovian fermions is to formulate the Lindblad master equation in the framework of non-equilibrium Keldysh field theory [41–43]. In this formalism, the evolution of the system is encoded in the partition function  $\mathcal{Z}$  defined on the Keldysh time contour  $\mathcal{C}$ ,

$$\mathcal{Z} = \int \prod_{i,\sigma} \mathcal{D}[c_{i\sigma}, \bar{c}_{i\sigma}] e^{i\mathcal{S}} \quad (4)$$

where  $\mathcal{S}$  is the Keldysh action. The latter is written in terms of the fermionic coherent state fields  $\{\bar{c}_{i\sigma\alpha}, c_{i\sigma\alpha}\}$ , which are defined on the forward ( $\alpha = +$ ) and backward ( $\alpha = -$ ) branches of the Keldysh contour for each lattice site  $i$  and spin  $\sigma$ :

$$\mathcal{S} = \int_{-\infty}^{+\infty} dt \sum_{\alpha=\{+,-\}} \sum_{i\sigma} \alpha \bar{c}_{i\sigma\alpha} i \partial_t c_{i\sigma\alpha} - i \int_{-\infty}^{+\infty} dt \mathcal{L} \quad (5)$$

The coherent and dissipative contributions to the dynamics are captured through the Lindbladian term  $\mathcal{L}$ , which in the Keldysh formalism becomes:

$$\mathcal{L} = -i(H_+ - H_-) + \sum_{i,\sigma} L_{i\sigma+} \bar{L}_{i\sigma-} - \frac{1}{2} (\bar{L}_{i\sigma+} L_{i\sigma+} + \bar{L}_{i\sigma-} L_{i\sigma-}) \quad (6)$$

In the infinite coordination limit, one can apply the cavity method: By isolating a single site (the "impurity") and integrating out the remaining lattice degrees of freedom, the influence of the surrounding sites is captured through a self-consistent bath, a frequency dependent non-Markovian environment which effectively encodes the feedback from the rest of the system. Therefore, in the infinite coordination limit the effective action

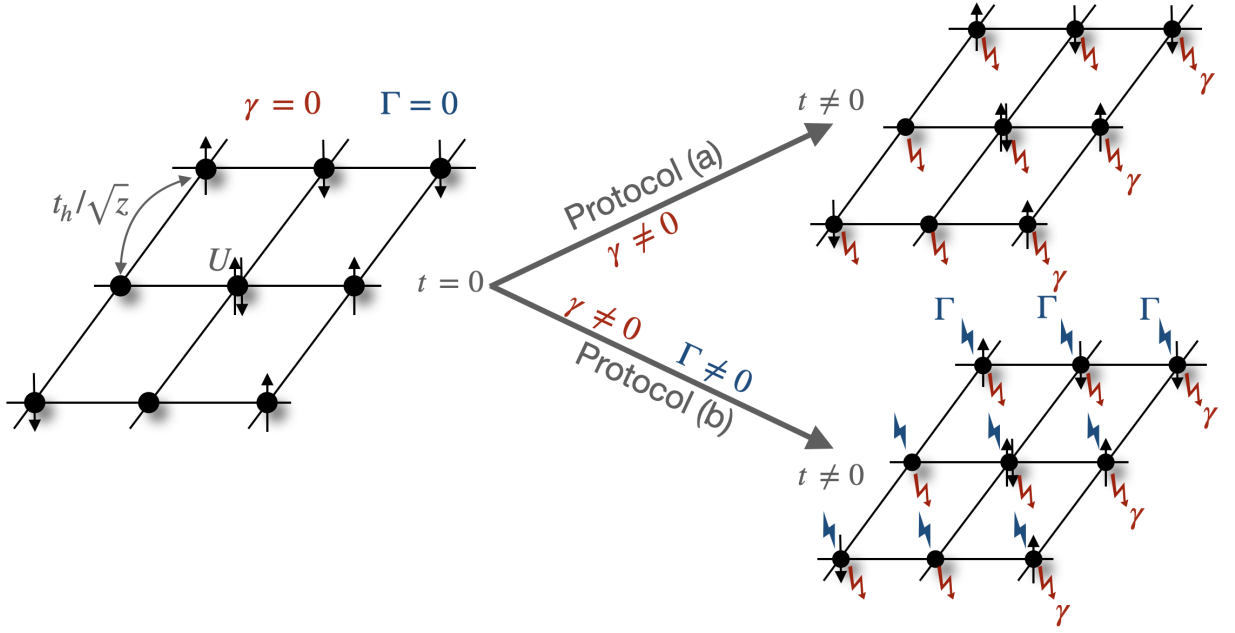


Figure 1. Quench protocol for the dissipative Fermi-Hubbard model — An interacting lattice system, characterized by the Coulomb interaction  $U$  and hopping amplitude  $t_h/\sqrt{z}$  at  $t = 0^+$  is subjected to a quench, involving either (a) Markovian dissipation alone ( $\gamma \neq 0$ ), or (b) both Markovian dissipation ( $\gamma \neq 0$ ) and photoexcitation ( $\Gamma \neq 0$ ).

of the impurity reads

$$\mathcal{S} = \mathcal{S}_{\text{loc}} - i \int_{\mathcal{C}} dt dt' \sum_{\sigma} \bar{c}_{\sigma}(t) \Delta_{\sigma}(t, t') c_{\sigma}(t'), \quad (7)$$

where  $\mathcal{S}_{\text{loc}}$  includes all local contributions coming from both coherent evolution (i.e. interactions) and dissipation, while  $\Delta_{\sigma}(t, t')$  is the hybridization function of the DMFT bath, which characterizes both the spectral properties and occupation of the effective bath. Within the DMFT framework, this hybridization function is determined self-consistently from the impurity Green's function,

$$G_{\sigma}(t, t') = -i \langle T_{\mathcal{C}} c_{\sigma}(t) c_{\sigma}^{\dagger}(t') \rangle \quad (8)$$

For a Bethe lattice with semi-elliptic density of states, the DMFT self-consistency condition closes in a simple analytic form [35], yielding to:

$$\Delta_{\sigma}(t, t') = t_h^2 G_{\sigma}(t, t') \quad (9)$$

Simulating the dynamics of the original dissipative Hubbard model within DMFT reduces to solving self-consistently the impurity problem defined by Eq. (7). In the present case this takes the form of a dissipative Anderson impurity model [38, 39] describing a single interacting spinful level with Coulomb repulsion and local dephasing. Below we detail the numerical approach used for the solution of the impurity problem and outline the physical observables extracted from it.

#### A. Impurity Solver and DMFT Self-consistent loop

We focus here on the impurity solver and the iterative numerical scheme for the DMFT self-consistency. We begin by defining the *non-interacting* (i.e., bath-decoupled) impurity Green's function  $G_{0,\sigma}(t, t')$ , which obeys the Dyson equation:

$$G_{0,\sigma}^{-1}(t, t') = [i\partial_t - H_{\text{loc},\sigma}(t)]\delta_{\mathcal{C}}(t, t'), \quad (10)$$

where  $H_{\text{loc},\sigma} = h_{\sigma}(t) + \epsilon_d - \mu$  denotes the local impurity Hamiltonian. It contains eventually the single-particle energy  $\epsilon_d$ , the chemical potential  $\mu$ , or the Hartree term  $h_{\sigma}(t) = U n_{\sigma}(t)$  with the density  $n_{\sigma}(t)$  per spin. In the present case we study a half-filled system, so that  $\mu = U/2$ ,  $\epsilon_d = 0$  and  $H_{\text{loc},\sigma}(t) = 0$ .

At the beginning we assume that the fully interacting impurity Green's function is simply given by  $G_0$ , and we calculate the hybridization  $\Delta$  with Eq. (9). Then, for each  $(t, t')$  in the Keldysh contour we solve the self-consistent DMFT loop:

1. The Weiss impurity Green's function  $\mathcal{G}$  is obtained by incorporating the hybridization of the bath via:

$$\mathcal{G}_{\sigma}^{-1}(t, t') = G_{0,\sigma}^{-1}(t, t') - \Delta_{\sigma}(t, t'), \quad (11)$$

where  $\Delta_{\sigma}(t, t')$  is the hybridization function obtained from the previous DMFT iteration or initial guess.

2. The full interacting impurity Green's function  $G_{\sigma}(t, t')$  is computed via the Dyson equation:

$$G_{\sigma}^{-1}(t, t') = \mathcal{G}_{\sigma}^{-1}(t, t') - \Sigma_{\text{int},\sigma}(t, t'), \quad (12)$$

where  $\Sigma_{\text{int},\sigma}(t, t')$  is the impurity self-energy, incorporating both coherent ( $\Sigma_{U,\sigma}$ ) and dissipative ( $\Sigma_{\gamma,\sigma}$ ) interaction:

$$\Sigma_{\text{int}}(t, t') \equiv \Sigma_{U,\sigma}(t, t') + \Sigma_{\gamma,\sigma}(t, t') \quad (13)$$

The Hubbard interaction term  $\Sigma_{U,\sigma}$  is computed using second-order iterated perturbation theory (IPT):

$$\Sigma_{U,\sigma}(t, t') = U(t)U(t') \mathcal{G}_\sigma(t, t') \mathcal{G}_{\bar{\sigma}}(t', t) \mathcal{G}_{\bar{\sigma}}(t, t'). \quad (14)$$

The purely dissipative part is captured through an additional local self-energy term

$$\Sigma_{\gamma,\sigma}(t, t') = \gamma G_\sigma(t, t) \delta(t, t'), \quad (15)$$

where  $\gamma$  denotes is local dephasing rate (see Appendix B for the derivation).

3. The updated Green's function  $G_\sigma(t, t')$  is then used to compute a new hybridization function via the DMFT self-consistency condition (9),

$$\Delta_\sigma(t, t') = t_h^2 G_\sigma(t, t') + \Gamma(t, t'), \quad (16)$$

where we introduced an additional contribution to the hybridization function,  $\Gamma(t, t')$ , in order to simulate a photo-excitation. This excitation is modeled as a pulse characterized by a duration  $T_0 = 1$  and an amplitude  $\Gamma$ , representing the strength of the coupling induced by the pulse. Details on the implementation of  $\Gamma(t, t')$  can be found in Appendix E.

The procedure is iterated until self-consistency is reached within a prescribed numerical tolerance. In summary, for each time argument  $(t, t')$  on the Keldysh contour, self-consistency is reached by iterating till convergence the following loop:

$$G_\sigma^{-1}(t, t') = [i\partial_t - H_{\text{loc}}(t)]\delta_C(t, t') - t_h^2 G_\sigma(t, t') - \Sigma_{\text{int},\sigma}(t, t') - \Gamma(t, t') \quad (17)$$

## B. Quantum Boltzmann Equation

When solving Dyson equations like Eq. (17), a major task is to obtain the Green's functions  $G(t, t')$  with their dependence on two time arguments from the many-body self-energy  $\Sigma(t, t')$  via the Kadanoff-Baym equations (KBE). The latter are equations of motion for  $G$ , in which  $\Sigma$  acts as a memory kernel. The main numerical cost is given by the evaluation of memory integrals, i.e., the convolution of  $G$  and  $\Sigma$  over earlier times. For an equidistant time discretization with  $N_t$  steps, the computational effort and the required computer memory shows a cubic scaling  $\mathcal{O}(N_t^3)$  and a quadratic scaling  $\mathcal{O}(N_t^2)$  with  $N_t$ , respectively. This represents a bottleneck for

studying the long-time heating dynamics of our electronic system. There are various paths to overcome this bottleneck [44]. Here we compute the time evolution of the system in Eq. (17) by means of a non-perturbative QBE for the energy distribution function

$$F(\omega, t) = \frac{\Im G^<(\omega, t)}{2\pi \mathcal{A}(\omega, t)} \quad (18)$$

solved in the framework of DMFT [45], where  $G^<$  is the lesser component of the interacting Green's function  $G$  and  $\mathcal{A}(\omega) = -\frac{1}{\pi} \Im G^R(\omega + i0)$  the spectrum and  $t$  is the average time. The QBE gives an equation

$$\partial_t F(\omega, t) = I_\omega[F(\omega, t), \cdot] \quad (19)$$

for the evolution of the electronic distribution function, with scattering integral:

$$I_\omega[F] = -i\{\Sigma^<(\omega, t) + \Sigma^R(\omega, t)F(\omega, t) - F(\omega, t)\Sigma^A(\omega, t)\} \quad (20)$$

where  $\Sigma(\omega, t) = \Sigma_{\text{int}}(\omega, t) + \Delta(\omega, t)$ . The evaluation of the functionals  $\Sigma_{\text{int}}(\omega, t)$  and  $\mathcal{A}(\omega, t)$  is done iteratively by solving a non-equilibrium steady-state (NESS) impurity problem with the suitable DMFT impurity solver. In practice, for each time  $t$ ,  $F(\omega, t+h) \equiv \bar{F}(\omega)$  is given by the QBE Eq. (19) and is not updated during the NESS loop described below, while  $\Sigma_{\text{int}}(\omega, t+h) \equiv \bar{\Sigma}_{\text{int}}(\omega)$  and  $\mathcal{A}(\omega, t+h) \equiv \bar{\mathcal{A}}(\omega)$  are calculated self-consistently in the following way:

1. Start from a guess for  $\bar{\Sigma}_{\text{int}}(\omega)$  (if you are at the very first timestep,  $t = 0$ , take for example the equilibrium  $\bar{\Sigma}_{\text{int}}$ , otherwise start from  $\bar{\Sigma}_{\text{int}}(\omega)$  calculated at the previous timestep) and solve the steady-state equation for  $\bar{G}^R(\omega)$ ,

$$\bar{G}^R(\omega) = [\omega + i0^+ - H_{\text{loc}}(t) - \bar{\Delta}^R(\omega) - \bar{\Sigma}_{\text{int}}^R(\omega)]^{-1}. \quad (21)$$

in order to determine  $\bar{\mathcal{A}}(\omega) = -\frac{1}{\pi} \Im \bar{G}^R(\omega + i0)$ . We recall that in our case (half-filling) it is always  $H_{\text{loc}}(t) = 0$ .

2. Determine the lesser Green's function from the given distribution function, using the steady-state variant of the fluctuation-dissipation theorem:

$$\bar{G}^<(\omega) = 2\pi i \bar{F}(\omega) \bar{\mathcal{A}}(\omega) \quad (22)$$

In NESS,  $\bar{F}(\omega)$  does not need to be a Fermi-Dirac distribution and, indeed, in general it is not.

3. Use the self-consistency Eq. (9) to fix the hybridization function of the effective steady state impurity model,

$$\bar{\Delta}^{R,<}(\omega) = t_h^2 \bar{G}^{R,<}(\omega) + \Gamma(\omega) \quad (23)$$

where  $\Gamma(\omega)$  is the additional contribution to the hybridization function that implement to simulate photoexcitation, see Appendix E.

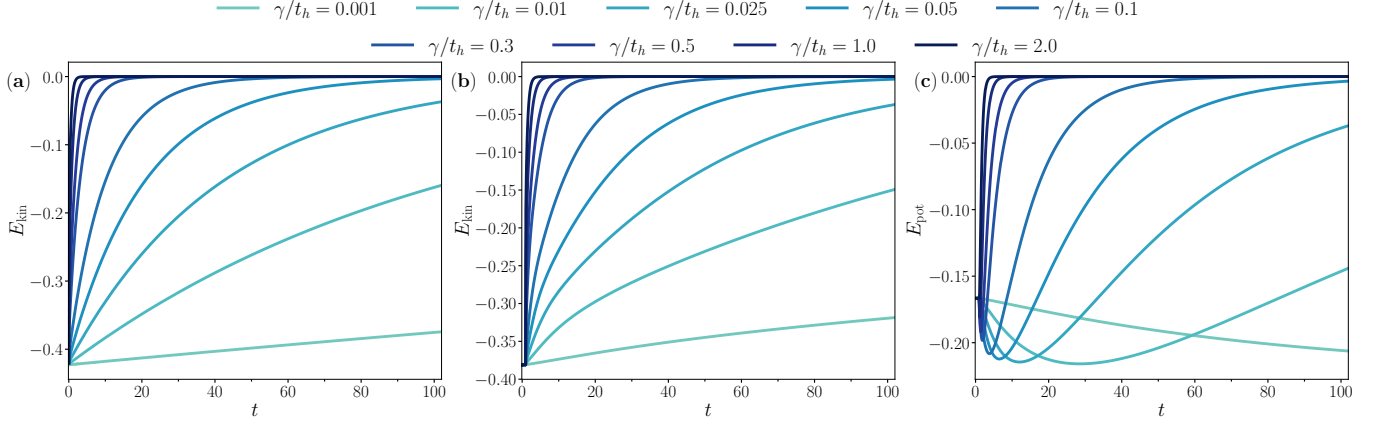


Figure 2. Dissipative Fermi-Hubbard Model - Dynamics of the kinetic and potential energy for increasing values of  $\gamma$ . Panel (a) shows the kinetic energy in the non-interacting Fermi-Hubbard model, where the potential energy is zero due to the absence of coherent interactions. Panels (b) and (c) show the kinetic and potential energy, respectively, for the interacting case with  $U/t_h = 2$ .

4. Solve the impurity model. With IPT as impurity solver, we first determine  $\bar{\mathcal{G}}(\omega)$  from  $\bar{\Delta}(\omega)$ ,

$$\begin{aligned}\bar{\mathcal{G}}^R(\omega) &= [\omega + i0^+ - H_{\text{loc}}(t) - \bar{\Delta}^R(\omega)]^{-1}, \\ \bar{\mathcal{G}}^<(\omega) &= \bar{\mathcal{G}}^R(\omega) \bar{\Delta}^<(\omega) \bar{\mathcal{G}}^A(\omega),\end{aligned}\quad (24)$$

then Fourier transform to relative time, evaluate the steady-state version of Eq. (14), and transform back to frequency space to obtain  $\bar{\Sigma}_U^{R,<}(\omega)$ .

5. In the time-translational invariant case (NESS loop), the purely dissipative part of the self-energy, Eq. (15), becomes

$$\bar{\Sigma}_\gamma^{R,<}(\omega) = \gamma(t) \frac{1}{2\pi} \int d\omega' \bar{G}^{R,<}(\omega') \quad (25)$$

6. Set  $\bar{\Sigma}_{\text{int}}(\omega) = \bar{\Sigma}_U(\omega) + \bar{\Sigma}_\gamma(\omega)$ , and iterate steps 1) to 5) until convergence.

The DMFT self-consistency serves as a way to evaluate  $\Sigma^{\text{NESS}}[F_G(\cdot, t)]$  (as well as  $\mathcal{A}^{\text{NESS}}[F_G(\cdot, t)]$  and  $\Delta^{\text{NESS}}[F_G(\cdot, t)]$ ). The differential equation (19) is then solved using a Runge-Kutta algorithm in fourth order, and, once  $F(\omega, t+h)$  is obtained, the new NESS loop at time  $t+h$  is solved.

The total energy of the system at (average) time  $t$  is

$$\begin{aligned}E_{\text{QBE}}(t) &= \frac{1}{2\pi} \int d\omega \{ -2i[\Delta_\sigma(\omega, t) G_\sigma(\omega, t)]^< \} \\ &+ \frac{1}{2\pi} \int d\omega \{ -i[\Sigma_{U,\sigma}(\omega, t) G_\sigma(\omega, t)]^< \} \quad (26)\end{aligned}$$

The non-perturbative QBE approach gives a computational effort which scales like  $\mathcal{O}(t_{\text{max}})$ , as compared to the  $\mathcal{O}(t_{\text{max}}^3)$  of the Noneq-DMFT solution. Moreover, in QBE the memory occupied does not depend on  $t_{\text{max}}$ , while in Noneq-DMFT it scales like  $\mathcal{O}(t_{\text{max}}^2)$ . The approximation on which the non-perturbative QBE relies

is the separation of timescales, i.e., the time evolution of the system has to be slow with respect to relevant internal energy differences in the system, such as the linewidth or relevant spectral features [45].

#### IV. RESULTS: QUENCH OF DISSIPATION

We now present our results for the dissipative dynamics of the Fermi-Hubbard model with dephasing, solved in the framework of the non-perturbative QBE with DMFT. The system is initialized at time  $t = 0^-$  in an interacting thermal state at temperature  $\beta_i = 20$ . At time  $t = 0^+$ , the dephasing rate  $\gamma$  is suddenly switched on, initiating the out-of-equilibrium dynamics.

##### A. Heating dynamics

We start by briefly discussing the dissipative but non-interacting case,  $U = 0$ , corresponding to a dissipative free fermion lattice system. We stress that due to the dephasing the system is still interacting, i.e non-gaussian in the dissipative sense. However the specific nature of the dissipation makes it possible to write the Green's function into a Dyson equation for the impurity solver (see Appendix C for more details). In Fig. 2 (a), we show the time evolution of the kinetic energy for increasing values of  $\gamma$ . We see that the kinetic energy increases exponentially towards zero,  $E_{\text{kin}} = 0$ , at long times for all values of  $\gamma$ . This exponential scaling is essentially characterized by a decay constant set by the dissipation rate. The steady-state value  $E_{\text{kin}} = 0$  is compatible with an infinite temperature state, as we will confirm later by looking at the distribution function and the effective temperature.



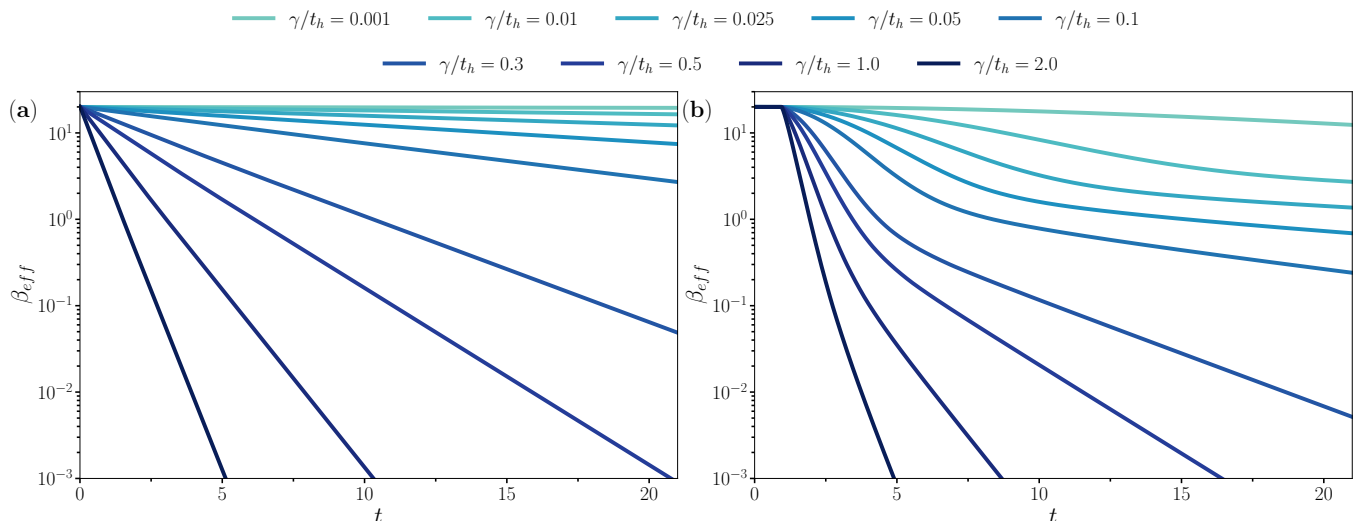


Figure 3. Dissipative Fermi-Hubbard Model - Dynamics of the effective temperature  $\beta_{\text{eff}}$  for increasing values of dephasing  $\gamma$ . Panel (a) shows the non-interacting case  $U/t_h = 0$ , while panel (b) displays the interacting case with  $U/t_h = 2$ . The initial temperature of the system is  $\beta_i = 20$ .

We now turn to the fully interacting regime and analyze the heating dynamics in the presence of local dephasing. Our goal is to highlight the role of interactions in shaping the relaxation behavior of the system. As shown in Fig. 2(b), the dynamics of the kinetic energy still reaches the infinite temperature regime for  $U/t_h = 2$ , however the thermalization timescale is strongly influenced by the interaction strength  $U$  and the dissipation rate  $\gamma$ . This becomes particularly evident in the weakly dissipative regime, where we see the kinetic energy firstly growing more rapidly at short times, and then slowing down for longer times. This behavior can be understood more clearly by examining the potential energy dynamics in Fig. 2(c). We observe an initial decrease in the potential energy, followed by a minimum at a characteristic time  $t^*$ , after which it begins to rise. The early-time decrease reflects the interplay between coherent interactions and dissipation, where the system initially tends to minimize its energy under the influence of  $U$  before dissipation becomes dominant. This intermediate regime, governed by the competition between coherent and dissipative processes, corresponds to the time window where the system exhibits a metastable prethermal plateau (see also Fig. 3(b) and the subsequent related discussion). However, at later times, dissipation begins to dominate and drives the system towards an infinite-temperature state, resulting in a monotonic increase in the potential energy as a function of time. The time  $t^*$  thus marks the crossover from interaction-dissipation dynamics to a purely dissipation-driven regime. While  $t^*$  scales approximately as  $t^* \propto 1/\gamma$  and remains almost independent of the interaction strength  $U$ , the potential energy at the crossover point  $E_{\text{pot}}(t^*)$  (not shown), decreases with increasing  $U$ , which leads to a more pronounced prethermal plateau at larger interaction strengths.

## B. Effective Temperature Dynamics

The emergence of infinite temperature thermalization is more clearly and unambiguously seen in the dynamics of the distribution function  $F(\omega, t)$  and in particular from its low-frequency component, which reflects the onset of an effective temperature. We extract a time-dependent effective temperature as  $F(\omega, t) \sim -\beta_{\text{eff}}(t)\omega/4$  around  $\omega = 0$  and plot  $\beta_{\text{eff}}$  as a function of time for different values of dephasing in Fig. 3. In absence of interactions, panel (a), the inverse effective temperature vanishes exponentially in time with a rate that grows with  $\gamma$ . For  $U/t_h = 2$  instead, as shown in panel (b), we see a different behavior. The dynamics of  $\beta_{\text{eff}}$  is at first faster, at short-times, due to interaction effects, and then slows down developing a prethermal plateau for weak values of dissipation. In particular, for  $\gamma/t_h < 0.025$ , the dynamics exhibits clear signatures of prethermalization: The effective temperature reaches a plateau and remains approximately constant over an extended time window, even as the total energy continues to evolve slowly. This decoupling of effective temperature and energy indicates the emergence of a long-lived prethermal state, which becomes more pronounced with increasing interaction strength, as larger values of  $U$  lead to longer-lived and more well-defined prethermal plateaus. For larger values of  $\gamma$ , dissipation quickly overcomes the effects of coherent interactions, making the system rapidly escape the prethermal plateau and relax exponentially fast toward the infinite-temperature limit.

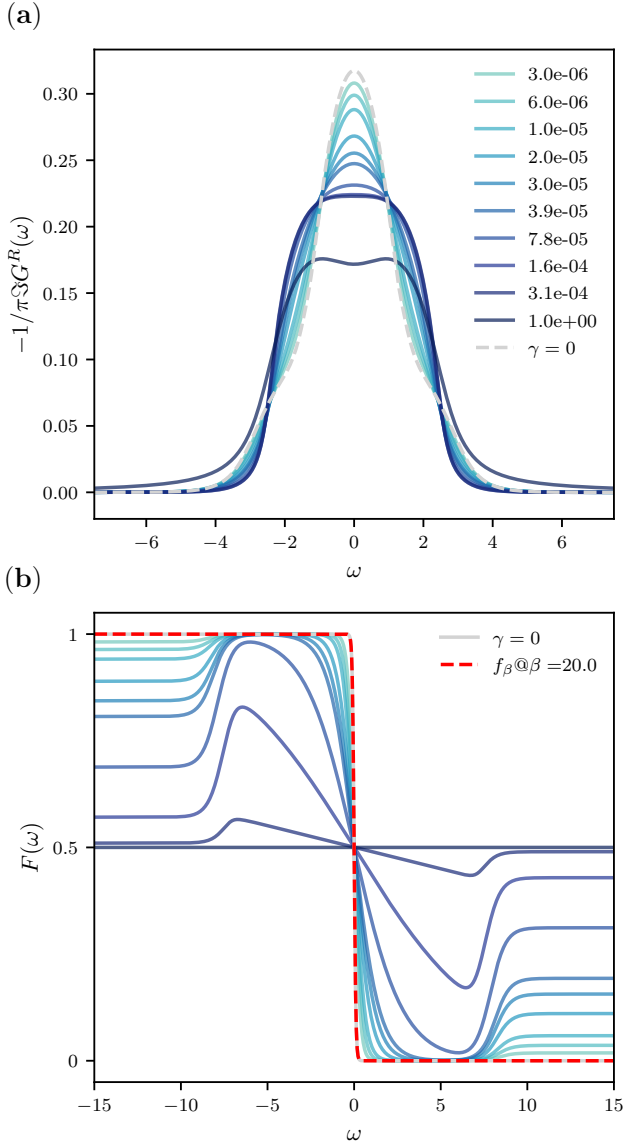


Figure 4. Dissipative Fermi-Hubbard Model - Spectral properties and distribution function of the interacting Fermi-Hubbard model ( $U/t_h = 2$ ) for increasing values of dephasing  $\gamma$  at  $t = 12500$ . Panel (a): Spectral function in the prethermal steady-state as a function of the dissipative rate  $\gamma$ . Panel (b): The corresponding distribution function, with the red dotted line showing the equilibrium fermi function at  $\beta_i = 20$  and  $\gamma = 0$ .

### C. Prethermal Steady-State Spectrum and Occupation

We then move to the steady-state which we characterize using the nonequilibrium Green's functions, in particular the spectrum and the occupation encoded in the retarded Green's function and in the distribution function. For moderate to high values of dephasing, the system approaches a genuine thermal state at infinite temperature

and as a result the distribution function becomes completely flat in frequency, see Fig. 4. The spectral function remains non-trivial; however, the coherent quasiparticle peak is destroyed by dissipation, and only broad, incoherent high-energy features corresponding to Hubbard bands remain visible in the spectrum. The situation at weak dephasing is, however, more interesting. We see in Fig. 4 that the prethermal steady-state features a highly non-thermal occupation. At low frequency we can still extract an effective temperature, as we did for the data in Fig. 3. Yet, we see that finite frequency excitations are not suppressed uniformly towards the infinite temperature state: in particular, the modes around the edge of the single particle bandwidth are the slowest to heat up.

Looking at the spectral function we see that the prethermal state looks like a correlated Fermi Liquid, with a local quasiparticle peak that is robust to weak dissipation and that melts down as  $\gamma$  increases. The transfer of spectral weight from low to high frequencies leads to an increase of the Hubbard bands, as already discussed.

## V. RESULTS: PHOTOEXCITATION

In this section we consider a different protocol, where the system is driven out of equilibrium via a photo-excitation and a simultaneous sudden switching of the dissipation  $\gamma$ . To simulate a photo-doping excitation, the system is transiently coupled to a fermionic bath with a suitably chosen spectral density. This in practice gives rise to an additional contribution to the electronic self-energy in terms of a kernel  $\Gamma(t, t')$

$$\Gamma(t, t') = V(t)G_{\text{bath}}(t, t')V(t')^*, \quad (27)$$

where  $V(t)$  is the time-dependent profile and  $G_{\text{bath}}$  the Green function of the fermionic bath (see Appendix E for more details concerning the excitation protocol). At the same time,  $t = 0^+$ , the dissipation  $\gamma$  is suddenly switched from  $\gamma = 0$  to  $\gamma \neq 0$ . This double excitation or double quench is often used for nonequilibrium problems [46–48]. It provides us with a knob to tune the degree in which the system is pushed out of equilibrium by a coherent or a dissipative perturbation, thus allowing to appreciate the interplay between the two processes.

In Fig. 5(a–c), we present the dynamics of the effective temperature for increasing values of the dissipation rate  $\gamma$  and photo-excitation amplitude  $\Gamma$ . We observe that when the dissipation rate is on the order of the photo-excitation amplitude, the effective temperature dynamics remain largely unchanged, meaning that the time scale of the dissipation is faster than the photo-excitation, which is confirmed by looking at the prethermal spectral function in Fig. 5(d–f). In contrast, when the dissipation rate is much smaller than the photo-excitation amplitude,  $\gamma \ll \Gamma$ , the dynamics become strongly dependent on  $\Gamma$ . Specifically, the dynamics accelerates as  $\Gamma$  increases. More notably, the prethermal plateau becomes

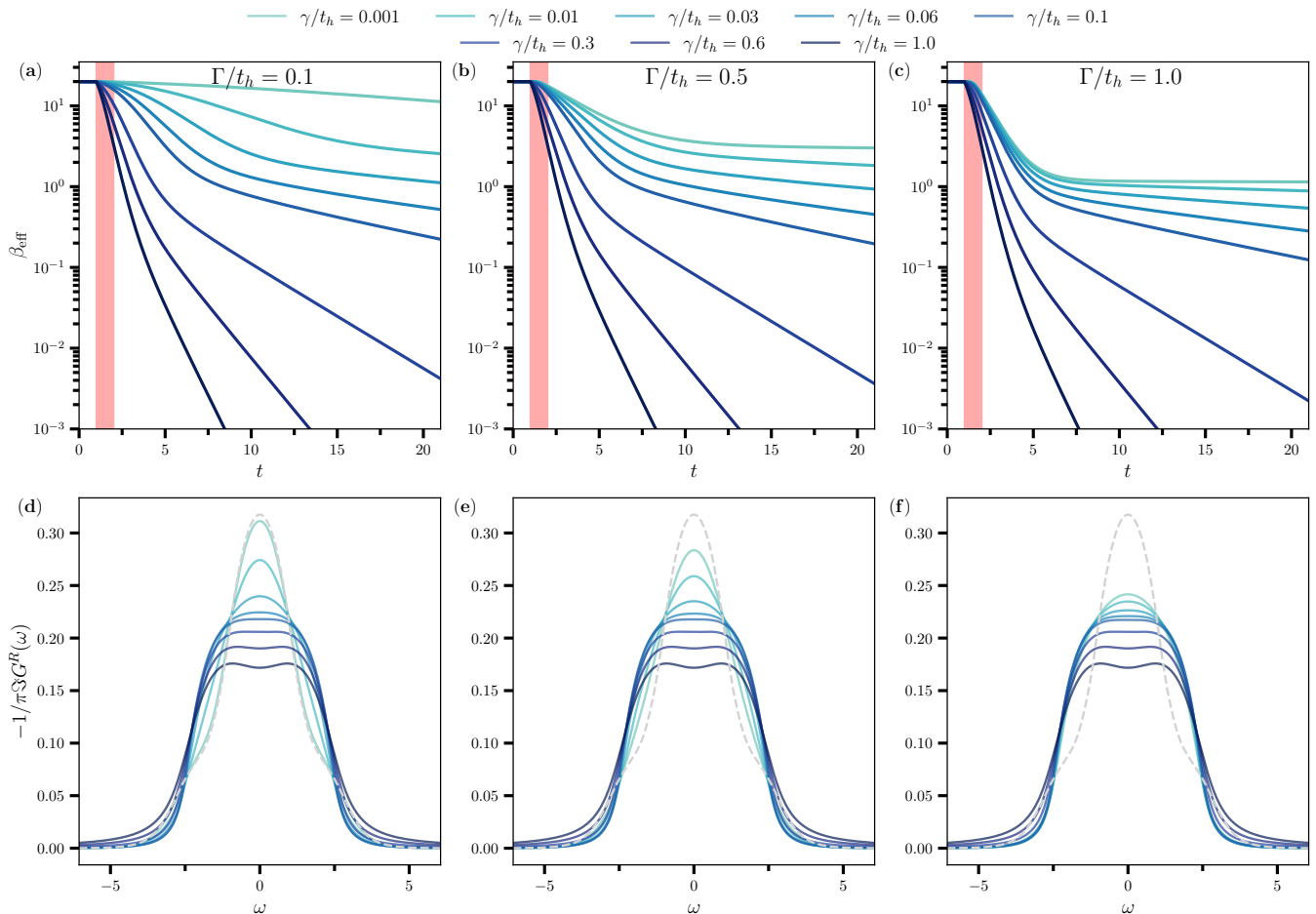


Figure 5. Dissipative Fermi-Hubbard Model under photo-excitation - (a-c) Dynamics of the effective temperature as a function of the dephasing rate  $\gamma$  for increasing value of photo-excitation amplitude  $\Gamma/t_h = 0.1, 0.5, 1.0$ . (d-f) corresponding prethermal spectral function, where the gray dot represents the non-dissipative case. Here the Coulomb interacting is fixed to  $U/t_h = 2$ .

more stable and persists over a longer time window compared to the case without photo-excitation, as illustrated in Fig. 3(b). Overall, these results confirm that, largely independently from the type of non-equilibrium excitation, the dissipative Fermi-Hubbard model thermalizes within DMFT to an infinite temperature state. The details of the protocol matter for what concerns the thermalization pathways, the timescales required to reach the infinite temperature steady-state, and the possible existence and lifetime of prethermal metastable states. In the next section, we take a closer look at how thermalization under open-system dynamics arises in DMFT.

## VI. EMERGENCE OF INFINITE TEMPERATURE THERMALIZATION

In this section we discuss more in detail how the onset of infinite temperature thermalization emerges within DMFT. To this extent we take advantage of recent progress in understanding thermalization of closed quan-

tum systems. In Ref. [40] we have shown that an interacting isolated quantum many-body system, such as the Fermi-Hubbard model, acts as *its own thermal bath* making local observables reach thermal equilibrium after a nonequilibrium perturbation. This process emerges naturally by looking at DMFT equation from a different perspective, the one in which the impurity is self-consistently updated together with the bath. In practice, instead of making the DMFT converge at each time step, we first evolve the dynamics of the impurity in a given bath up to long times. Then, by imposing the self-consistency, we obtain the new bath for the next iteration  $n$  (see Appendix D for further details). This amounts, in practice, in exchanging the order of limits between  $t \rightarrow \infty$  (long-time limit) and  $n \rightarrow \infty$  (DMFT self-consistency).

This analysis, applied to an isolated system evolving unitarily, revealed the emergence of a sharp *thermalization front* in the plane  $(n, t)$  separating the initial state (where the memory of the initial condition is) from the full thermal state [40]. This has a simple interpretation: under a local perturbation the impurity at long-times al-



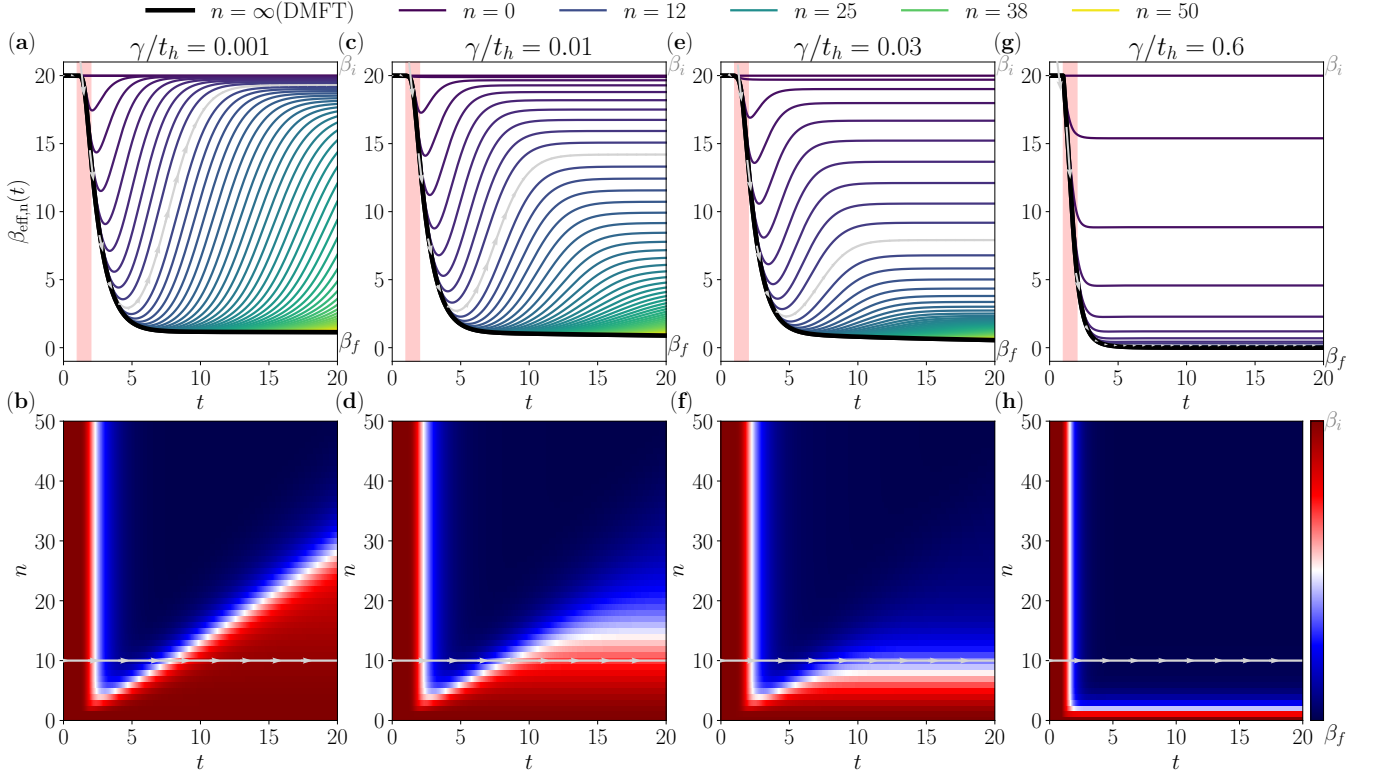


Figure 6. Thermalization Front of the Dissipative Hubbard Model for the Effective Temperature - Panel (a-h) describes the dynamics of the effective temperature for each iteration  $n$  and for different values of dephasing  $\gamma/t_h = 0.001, 0.01, 0.03, 0.6$ , compared to the fully self-consistent DMFT solution (black line) as obtained with QBE. We see clearly that contrary to the unitary Hubbard model, the effective temperature do not goes back to the initial value for all the iteration  $n$ , but reaches a non-thermal steady-state at  $\beta_{\text{eff},n} < \beta_i$ . This non-thermal steady-state act as a cut-off of the thermalization front. Here the photo-excitation amplitude is fixed at  $\Gamma/t_h = 1$ .

ways thermalizes back to the temperature of the bath, i.e. the initial temperature; still, the DMFT self-consistency heats up the bath more and more as  $n$  increases, by propagating a thermal wave from short to long times.

We now use the same approach for our dissipative Hubbard model with dephasing, namely we solve the DMFT equations step by step following the bath as it adapts to the impurity and viceversa, with the goal of understanding how the DMFT self-consistency allows the lattice model to heat up to infinite temperature.

In Fig. 6(a-g, top panels), we show the dynamics of the effective temperature  $\beta_{\text{eff}}$  at different DMFT iteration steps, and for increasing values of the dephasing rate  $\gamma/t_h = 0.001, 0.01, 0.03, 0.6$  (from left to right). These results are compared to the fully converged DMFT solution ( $n = \infty$ ), shown with a dark full line.

For very weak dissipation,  $\gamma/t_h = 0.001$ , we see that the effective temperature decreases in time (following essentially the fully converged DMFT solution), then reaches a minimum and starts increasing, going back to a value which is very close to the initial one. If we plot these data in the  $n, t$  plane (see bottom panels) we see clearly a sharp thermalization front with a linearly dispersing edge, characteristic of ballistic spreading, in accordance

with the results of the unitary case [40]. As we increase the value of the dephasing however we see a qualitative change in this picture. Notably, we see that at long times the effective temperature  $\beta_{\text{eff},n}(t)$  after each DMFT iteration does not reach the same initial value. Rather it stabilizes into a plateau value corresponding to a final temperature  $\beta_f < \beta_{\text{eff},n} < \beta_i$ , where  $\beta_i$  and  $\beta_f$  are the initial and final inverse temperatures of the full-DMFT solution, shown in the top panels of Fig. 6. As the DMFT self-consistency is iterated this plateau value decreases with  $n$ , ultimately reaching  $\beta_{\text{eff},n} \sim \beta_f$  for  $n \rightarrow \infty$ . We note that for non-interacting dissipative fermions the approach with  $n$  is clearly exponential, while in presence of interaction one can see a richer behavior with metastable states (see Appendix F). As a result, we see that the sharp thermalization front gets strongly affected by dissipation, first bending and flattening as  $\gamma$  increases and ultimately completely disappearing for sufficiently large dephasing (see panel h).

We can understand this phenomenology by thinking again at the physics of the (dissipative) quantum impurity model onto which the Fermi-Hubbard model with dephasing is mapped. Here the dephasing acts only on the impurity site, which is also coupled to the non-Markovian

DMFT bath. As such, from the point of view of the impurity, dephasing is not sufficient to drive the system towards infinite temperature nor it is enough to allow the system to thermalize back to the temperature of the bath as it was the case for the unitary case. As a result the dissipative quantum impurity model sets itself into a nonequilibrium steady-state, resulting from the simultaneous coupling with two different environments, leading to a finite effective temperature. Upon increasing  $n$ , as the DMFT bath is made more and more self-consistent by adjusting the bath spectrum to the local impurity Green's function, the impurity is heat up more and more and the next step effective temperature increases up to the point in which  $\beta_{\text{eff},n} \rightarrow 0$ . Increasing the value of the dephasing makes the process of thermalization to a nonequilibrium steady state more efficient and fast and makes the memory of the initial condition fade away more rapidly, with the result that the front bends more and more and ultimately disappears. We conclude therefore that for dissipative system thermalization does not arise as a thermal front, characterised by a memory of the initial condition, but rather as a single step process. This is reasonable since the Lindblad dynamics involves irreversibility and does not retain memory of the initial condition. Our results therefore confirm that this approach captures some key feature of the nonequilibrium dynamics.

We close by noting that this thermalization front and its lack of at strong dephasing is a direct consequence of having a perturbation acting on the unitary part of the evolution, in our case the photo-excitation. Indeed when only the dephasing is quenched, the non-reversible nature of the dissipation leads to a monotonic decrease in the effective temperature over time, eventually reaching a prethermal plateau at  $\beta_{\text{eff},n}$ . We expect that performing a quench in the interaction, instead of photoexcitation, would lead to qualitatively similar results.

## VII. CONCLUSIONS

In this work we have studied a dissipative Fermi-Hubbard model with dephasing and discuss the dynamics of thermalization and heating due to dissipation. We have solved the many-body Lindblad dynamics using nonequilibrium DMFT, corresponding to take the infinite connectivity limit of the lattice problem and solving a self-consistent dissipative quantum impurity model. The latter in the present case takes the form of a dissipative Anderson impurity model with dephasing, which we have solved with weak-coupling perturbation theory. We have focused on two different nonequilibrium protocols, corresponding to (i) a pure quench of the dissipation and (ii) a simultaneous photo-excitation and dissipation quench.

We have discussed the heating dynamics of the system, as described by the kinetic and potential energy as well as the effective temperature, which show thermalization towards an infinite temperature state. We have

shown that the heating rates depend strongly on interaction and dephasing. In particular, for the case of dissipation quench we have shown the emergence of a prethermal regime for weak dissipation, where a quasi-stationary state is formed before heating dominates at long times. This prethermal steady state is shown to still display coherent quasiparticles and a quasi-equilibrium distribution function at low energy, while high-frequency excitations are non-thermally occupied. The dynamics under protocol (ii) corresponding to simultaneous photo-excitation and dephasing display similar features, with the addition that the strength of the photodoping has the effect of stabilizing a prethermal plateau for weak dissipation.

Finally we have studied how thermalization to infinite temperature arises from the point of view of the impurity, or equivalently how the many-body system acts as its own thermal bath, using recent insights obtained from the closed system case. We have shown that the thermalization front emerging in the unitary case is strongly modified by dissipation, a signature of the irreversibility of the open system dynamics. In particular, while for weak dephasing a linear front remains visible, for moderate and large values of dissipation the front bends and flatten out, a signature of the fact that the thermalization dynamics becomes completely dominated by the dissipative processes.

In the future it would be interesting to explore the effect of different types of dephasing mechanism, as done for the impurity model in Refs. [38, 39], as well as the regime of strong interaction and strong dissipation, where the perturbative approach used in this work would not work.

## ACKNOWLEDGMENTS

We thank Denis Golež for valuable and stimulating discussions. We acknowledge financial support from the ERC consolidator Grant No. 101002955 - CONQUER. A. P. acknowledges funding from the European Union's Horizon 2020 research and innovation programme under the Marie Skłodowska-Curie Postdoctoral Fellowship (Grant Agreement No. 101149691 - DISRUPT). We are grateful for the use of computational resources from the Collège de France IPH cluster. A. P. is grateful to Philipp Hansmann and the RRZE of the University of Erlangen-Nuremberg for providing additional computational resources.

## Appendix A: From Lindblad to Out-of-Equilibrium DMFT

We present here the formalism of DMFT for Markovian dissipation. As already explained in the main text, the starting point to derive non-equilibrium DMFT equations for Markovian systems is to cast the Lindblad master equation (1) in the language of non-equilibrium

Keldysh field theory, given the Hubbard Hamiltonian (2) and the local jump operators in Eq. (3). In this formalism, the evolution of the system is encoded in the partition function  $\mathcal{Z}$  in Eq. (4), with the Keldysh action (5). The coherent and dissipative contributions to the dynamics are captured through the Lindbladian term  $\mathcal{L}$  in Eq. (6). We split the action  $\mathcal{S}$  in Eq. (5) into three parts,

$$\mathcal{S} = \mathcal{S}_{\text{loc}} + \delta\mathcal{S} + \mathcal{S}_{(0)} \quad (\text{A1})$$

where the first contribution  $\mathcal{S}_{\text{loc}}$  corresponds to the part of the action, that only contains grassmann at site  $i = 0$ ,

$$\begin{aligned} \mathcal{S}_{\text{loc}} = & \int dt \sum_{\alpha\sigma} \alpha (\bar{c}_{0\sigma\alpha} i \partial_t c_{0\sigma\alpha} - U n_{0\uparrow\alpha} n_{0\downarrow\alpha}) \\ & - i \left( \sum_{\sigma} L_{0\sigma+} \bar{L}_{0\sigma-} - \frac{1}{2} (\bar{L}_{0\sigma+} L_{0\sigma+} + \bar{L}_{0\sigma-} L_{0\sigma-}) \right) \end{aligned} \quad (\text{A2})$$

Then the second term  $\delta\mathcal{S}$  takes into account the hopping between the site  $i = 0$  and the other sites of the lattice,  $i \neq 0$ ,

$$\delta\mathcal{S} = -\frac{t_h}{\sqrt{z}} \int dt \sum_{\alpha\sigma} \sum_{\langle 0,j \rangle} \alpha (\bar{c}_{0\sigma\alpha} c_{j\sigma\alpha} + \bar{c}_{j\sigma\alpha} c_{0\sigma\alpha}) \quad (\text{A3})$$

Finally the last contribution  $\mathcal{S}_{(0)}$  is the part of the action where the site  $i = 0$  and its bonds are removed ( $i, j \neq 0$ )

$$\begin{aligned} \mathcal{S}_{(0)} = & \int dt \sum_{\alpha\sigma} \sum_{i \neq 0} \alpha [\bar{c}_{i\sigma\alpha} i \partial_t c_{i\sigma\alpha} - \alpha H_{(0)\alpha}] \\ & - i \sum_{i \neq 0, \sigma} L_{i\sigma+} \bar{L}_{i\sigma-} - \frac{1}{2} (\bar{L}_{i\sigma+} L_{i\sigma+} + \bar{L}_{i\sigma-} L_{i\sigma-}) \end{aligned} \quad (\text{A4})$$

with  $H_{(0)}$  the Hamiltonian defined as,

$$H_{(0)} = -\frac{t_h}{\sqrt{z}} \sum_{\langle i,j \rangle, i,j \neq 0, \sigma} (c_{i\sigma}^\dagger c_{j\sigma} + c_{j\sigma}^\dagger c_{i\sigma}) + \sum_{i \neq 0} U n_{i,\uparrow} n_{i,\downarrow} \quad (\text{A5})$$

The first step of the derivation is to rewrite the partition function  $\mathcal{Z}$  in terms of the three contributions of the Keldysh action,

$$\begin{aligned} \mathcal{Z} = & \int \prod_{i,\sigma} \mathcal{D}[c_{i\sigma}, \bar{c}_{i\sigma}] e^{i\mathcal{S}} \\ = & \int \prod_{\sigma} \mathcal{D}[c_{0\sigma}, \bar{c}_{0\sigma}] e^{i\mathcal{S}_{\text{loc}}} \int \prod_{i \neq 0, \sigma} \mathcal{D}[c_{i\sigma}, \bar{c}_{i\sigma}] e^{i\mathcal{S}_{(0)}} e^{i\delta\mathcal{S}} \end{aligned} \quad (\text{A6})$$

We now introduce the contour-ordered expectation value with respect to the action  $\mathcal{S}_{(0)}$ ,

$$\langle X \rangle_{(0)} = \frac{1}{\mathcal{Z}_{(0)}} \int \prod_{i \neq 0, \sigma} \mathcal{D}[c_{i\sigma}, \bar{c}_{i\sigma}] X e^{i\mathcal{S}_{(0)}} \quad (\text{A7})$$

where  $\mathcal{Z}_{(0)}$  is the corresponding partition function of the decoupled lattice. Using this relation, the full partition function can be recast as

$$\mathcal{Z} = \mathcal{Z}_{(0)} \int \prod_{\sigma} \mathcal{D}[c_{0\sigma}, \bar{c}_{0\sigma}] e^{i\mathcal{S}_{\text{loc}}} \langle e^{i\delta\mathcal{S}} \rangle_{(0)} \quad (\text{A8})$$

By using a cumulant expansion, we can formally rewrite the expectation value  $\langle e^{i\delta\mathcal{S}} \rangle_{(0)}$  as,

$$\begin{aligned} \langle e^{i\delta\mathcal{S}} \rangle_{(0)} = & \exp [\langle i\delta\mathcal{S} \rangle_{(0)} \\ & + \frac{1}{2} (\langle [i\delta\mathcal{S}]^2 \rangle_{(0)} - [\langle i\delta\mathcal{S} \rangle_{(0)}]^2) + \dots] \end{aligned} \quad (\text{A9})$$

with,

$$\begin{aligned} \langle (i\delta\mathcal{S})^2 \rangle_{(0)} = & 2 \int d\tau \int d\tau' \sum_{\alpha\beta} \alpha\beta \\ & \sum_{\sigma} \bar{c}_{0\sigma\alpha}(t_1) \left[ \sum_{j,k \neq 0} \frac{t_h^2}{z} G_{jk,\sigma}^{\alpha\beta,(0)}(t_1, t_2) \right] c_{0\sigma\beta}(t_2) \end{aligned} \quad (\text{A10})$$

where we defined the Green's function  $G_{jk,\sigma}^{\alpha\beta,(0)}$  as,

$$G_{jk,\sigma}^{\alpha\beta,(0)}(t, t') = -i \langle T_C c_{j\sigma\alpha}(t) \bar{c}_{k\sigma\beta}(t') \rangle_{(0)} \quad (\text{A11})$$

with  $T_C$  the time-ordering operator along the Keldysh contour.

The central idea of dynamical mean-field theory (DMFT) is to derive an effective Keldysh action for the fermionic degrees of freedom on a single lattice site (the "impurity") by integrating out all other sites in the system, thus mapping the fully interacting lattice model onto a single interacting impurity coupled to a self-consistently determined quantum bath. In the large connectivity limit,  $z \gg 1$ , one can expand the action in power of  $1/z$ , obtain the effective Keldysh action, and write it in closed form as,

$$\begin{aligned} \mathcal{S}_{\text{eff}} [\bar{c}_{0\sigma\alpha}, c_{0\sigma\alpha}] = & \log \int \prod_{i \neq 0} \mathcal{D}[\bar{c}_{i\sigma}, c_{i\sigma}] e^{i\mathcal{S}} \\ = & \mathcal{S}_{\text{loc}} - i \sum_{\sigma} \sum_{\alpha\beta} \alpha\beta \int dt dt' \bar{c}_{0\sigma\alpha}(t) \Delta_{\sigma}^{\alpha\beta}(t, t') c_{0\sigma\beta}(t') \end{aligned} \quad (\text{A12})$$

In this expression,  $\mathcal{S}_{\text{loc}}$  is the local on-site contribution of the original lattice action Eq. (5), which includes interactions and possible dissipation. The second term captures the influence of the rest of the lattice on the impurity site via an effective non-Markovian bath characterized by the hybridization function  $\Delta_{\sigma}^{\alpha\beta}$  which is given by:

$$\Delta_{\sigma}^{\alpha\beta}(t, t') = \sum_{j,k \neq 0} \frac{t_h^2}{z} G_{jk,\sigma}^{(0),\alpha\beta}(t, t') \quad (\text{A13})$$

To close the DMFT loop, one must impose a self-consistency condition that relates observables computed

from the cavity action to those obtained from the effective impurity action (A12). The specific form of this condition depends on the lattice geometry. For the Bethe lattice this relation becomes especially simple, as the removal of a site fully decouples its neighbors. In this case, the off-diagonal cavity Green's functions vanish, and we obtain:

$$G_{jk,\sigma}^{(0)}(t, t') = \delta_{j,k} G_{jk,\sigma}^{S_{\text{eff}}}(t, t') \quad (\text{A14})$$

Using this, the hybridization function simplifies to

$$\Delta_{\sigma}^{\alpha\beta}(t, t') = \frac{t_h^2}{z} G_{\sigma}^{S_{\text{eff}}, \alpha\beta}(t, t') \quad (\text{A15})$$

which directly relates the hybridization function of the non-Markovian bath to the interacting Green's function of the impurity,

$$G_{\sigma}^{S_{\text{eff}}, \alpha\beta}(t, t') = -i \langle c_{0\sigma\alpha}(t) \bar{c}_{0\sigma\beta}(t') \rangle_{S_{\text{eff}}} \quad (\text{A16})$$

Solving the original dissipative and interacting lattice problem within DMFT thus amounts to self-consistently solving the impurity problem defined by the effective Keldysh action (A12), computing the corresponding impurity Green's function (A16), and updating the hybridization function via Eq. (A15) until convergence is achieved.

## Appendix B: Derivation of the Dissipative Self-Energy

In the previous section, we demonstrated that in the limit  $z \rightarrow \infty$ , the fully interacting and dissipative Hubbard model can be exactly mapped onto a dissipative quantum impurity model. Building on this result, we now focus on the dissipative part of self-energy for the non-interacting impurity solver. As a starting point, we consider the partition function of the impurity model, which takes the form,

$$\mathcal{Z} = \int \mathcal{D}[c, \bar{c}] \exp \{i\mathcal{S}_{\text{free}} + i\mathcal{S}_{\gamma}\} \quad (\text{B1})$$

where  $\mathcal{S}_{\text{free}}$  denotes the action of the non-dissipative impurity model, and  $\mathcal{S}_{\gamma}$  represents the dissipative contribution, which we recall is given by:

$$\mathcal{S}_{\gamma} = -i \left[ \int d\tau \sum_{\sigma} \gamma n_{\sigma+} n_{\sigma-} - \frac{\gamma}{2} n_{\sigma+} - \frac{\gamma}{2} n_{\sigma-} \right] \quad (\text{B2})$$

where  $n_{\sigma,\pm} = c_{\sigma,\pm}^{\dagger} c_{\sigma,\pm}$  are the number operators of the impurity on the forward (+) and backward (-) branches of the Keldysh contour, respectively. From this partition function, the interacting impurity Green's function is defined as the contour-ordered expectation value

$$\begin{aligned} G_{\sigma}^{\alpha\beta}(t, t') &= -i \langle \mathcal{T}_C c_{\sigma\alpha}(t) c_{\sigma\beta}^{\dagger}(t') \rangle_{S=S_{\text{free}}+S_{\gamma}} \\ &= -i \int \mathcal{D}[\psi, \bar{\psi}] c_{\sigma\alpha}(t) c_{\sigma\beta}^{\dagger}(t') e^{i\mathcal{S}_{\text{free}}+i\mathcal{S}_{\gamma}} \end{aligned} \quad (\text{B3})$$

By using a standard Taylor expansion for the dissipative action  $\mathcal{S}_{\gamma}$ , we can write all the order of the Green's function,

$$G_{\sigma}^{\alpha\beta}(t, t') = -i \int \mathcal{D}[\psi, \psi^*] e^{i\mathcal{S}_{\text{free}}} c_{\sigma\alpha}(t) c_{\sigma\beta}^{\dagger}(t') [1 + i\mathcal{S}_{\gamma} + \dots] \quad (\text{B4})$$

which serves as a starting point for a perturbative treatment of the dissipation within the impurity problem.

### 1. Perturbative expansion in terms of $\gamma$

At first order in the dissipation strength  $\gamma$ , the correction to the Green's function can be decomposed into two distinct contributions,

$$G_{\sigma}^{(1)\alpha\beta}(t, t') = G_{\sigma, \text{jump}}^{(1)\alpha\beta}(t, t') + G_{\sigma, \text{NH}}^{(1)\alpha\beta}(t, t') \quad (\text{B5})$$

where  $G_{\sigma, \text{jump}}^{(1)\alpha\beta}$  arises from the quantum jump terms, and  $G_{\sigma, \text{NH}}^{(1)\alpha\beta}$  originates from the non-Hermitian part of the dissipative action. These contributions are explicitly given by,

$$\begin{aligned} G_{\sigma, \text{jump}}^{(1)\alpha\beta}(t, t') &= \gamma \int d\tau \left[ -\mathcal{G}_{\sigma}^{\alpha+}(t, \tau) \mathcal{G}_{\sigma}^{-+}(\tau, \tau) \mathcal{G}_{\sigma}^{+\beta}(\tau, t') \right. \\ &\quad - \mathcal{G}_{\sigma}^{\alpha-}(t, \tau) \mathcal{G}_{\sigma}^{++}(\tau, \tau) \mathcal{G}_{\sigma}^{-\beta}(\tau, t') \\ &\quad + \mathcal{G}_{\sigma}^{\alpha+}(t, \tau) \mathcal{G}_{\sigma}^{+-}(\tau, \tau) \mathcal{G}_{\sigma}^{-\beta}(\tau, t') \\ &\quad \left. + \mathcal{G}_{\sigma}^{\alpha-}(t, \tau) \mathcal{G}_{\sigma}^{-+}(\tau, \tau) \mathcal{G}_{\sigma}^{+\beta}(\tau, t') \right] \end{aligned} \quad (\text{B6})$$

and

$$G_{\sigma, \text{NH}}^{(1)\alpha\beta}(t, t') = \gamma \sum_{\alpha_1=+,-} \int d\tau \mathcal{G}_{\sigma}^{\alpha\alpha_1}(t, \tau) \mathcal{G}_{\sigma}^{\alpha_1\beta}(\tau, t') \quad (\text{B7})$$

where we have used the Wick's theorem, since the non-dissipative part of the action  $\mathcal{S}_{\text{free}}$  is quadratic. By summing all first-order contributions, we obtain the full correction  $G_{\sigma}^{(1)\alpha\beta}$  including the (++) component as well as all other Keldysh components. From this result, the first-order correction to the self-energy can be extracted via direct comparison with the Dyson equation,

$$\Sigma_{\gamma\sigma}^{(1)}(t, t') = \gamma \mathcal{G}_{\sigma}(t, t) \delta(t - t') \quad (\text{B8})$$

In the same spirit, the second-order correction to the self-energy can be computed using higher-order terms in the perturbative expansion. Remarkably, for the specific choice of local dephasing considered here, it has been shown that the entire perturbative series can be resummed. This resummation yields an exact expression for the dissipative part of the self-energy, which takes a closed form [38, 49],

$$\Sigma_{\gamma\sigma}(t, t') = \gamma G_{\sigma}(t, t) \delta(t - t') \quad (\text{B9})$$

## Appendix C: Non-interacting Fermi-Hubbard Model

Now that we have derived the dissipative part of the self-energy, we can analyze the exact dynamics of the non-interacting ( $U = 0$ ) dissipative Hubbard model. Even in the absence of Coulomb interactions, the system remains non-Gaussian due to the structure of the dissipation, which can lead to nontrivial dynamics and non-equilibrium steady state. We start by considering the Dyson equation defined in Eq. (12)

$$G_{\sigma}^{-1}(\omega) = \omega - \Delta_{\sigma}(\omega) - \Sigma_{\text{int},\sigma}(\omega) \quad (\text{C1})$$

where in this case the interacting self-energy is only given by the dissipative part  $\Sigma_{\text{int},\sigma}(\omega) = \Sigma_{\gamma\sigma}(\omega)$  defined in Eq. (25). As discussed in the main text, we are considering the Bethe lattice with  $t_h = 1$ , such that the hybridization function satisfies

$$\Delta_{\sigma}(t, t') = t_h^2 G_{\sigma}(t, t') \quad (\text{C2})$$

Inserting (C2) in (C1) yields

$$G_{\sigma}(\omega) = \frac{1}{\omega - \epsilon_d - t_h^2 G_{\sigma}(z) - \Sigma_{\gamma\sigma}(z)} \quad (\text{C3})$$

which is the DMFT equation for the non-interacting but dissipative Hubbard model.

### 1. Analytical expression of the Retarded Green's Function

From Eq. (C3), the simple structure of the dissipative self-energy  $\Sigma_{\gamma\sigma}(\omega)$ , allows us to derive an exact analytical expression for the retarded Green's function. Specifically, for the retarded component, the DMFT equation takes the form:

$$G_{\sigma}^R(\omega) = \frac{1}{\omega + i\eta - t_h^2 G_{\sigma}^R(\omega) + i\frac{\gamma}{2}} \quad (\text{C4})$$

where we have introduced  $\eta \rightarrow 0^+$  and we have used the fact that  $\Sigma_{\gamma\sigma}(\omega) = -i\gamma/2$ . The resulting expression can be formally rewritten in polynomial form:

$$[G_{\sigma}^R(\omega)]^2 - \frac{z + i\frac{\gamma}{2}}{t_h^2} G_{\sigma}^R(\omega) + \frac{1}{t_h^2} = 0 \quad (\text{C5})$$

whose solutions can be obtained analytically as,

$$G^R(\omega) = \frac{1}{t_h^2} \left[ \left( \omega + i\eta + i\frac{\gamma}{2} \right) \pm \sqrt{\left( \omega + i\eta + i\frac{\gamma}{2} \right)^2 - 4t_h^2} \right] \quad (\text{C6})$$

In the same spirit, we can derive an analytical expression for the Keldysh component of the Green's function, at least in the half-filling case, since dephasing does not break particle-hole symmetry.

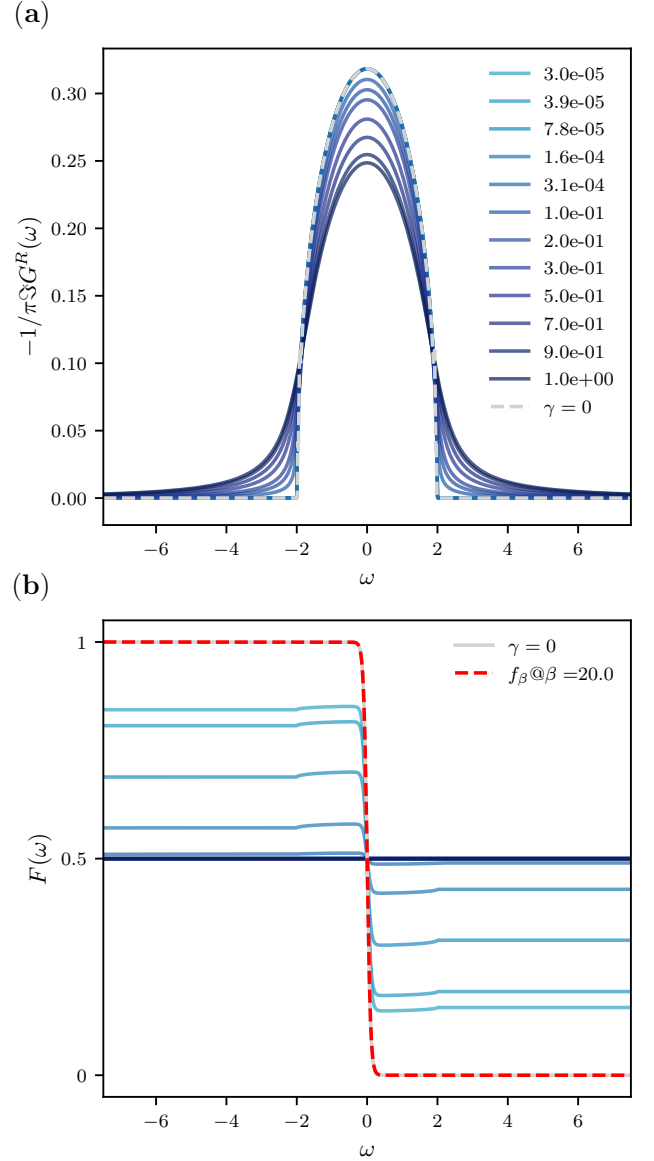


Figure 7. Dissipative Fermi-Hubbard Model - Spectral properties and distribution function of the non-interacting Fermi-Hubbard model ( $U/t_h = 0$ ) for increasing values of dephasing  $\gamma$  at  $t = 12500$ . Panel (a) Spectral function in the prethermal steady-state as a function of the dissipative rate  $\gamma$ . Panel (b) shows the corresponding distribution function, with the dot red line the equilibrium fermi function at  $\beta_i = 20$ .

### 2. Steady-State Spectrum and Occupation

We now turn our attention on the spectral function and the distribution function of the non-interacting dissipative Hubbard model, that we show in Fig. 7, for increasing values of dephasing rate  $\gamma$ . As  $\gamma$  increases, we see that the typical resonance of the bethe lattice is broadened and at the same time the value at  $\omega = 0$  decreases with  $\gamma$ , which is a signature of loss of coherence due to the



Markovian environment. At the same time, the distribution function deviates from the equilibrium Fermi-Dirac form, reflecting the fact that the system is driven out of equilibrium and relaxes to a prethermal state. Importantly, it's seem that the dissipation act almost uniformly across all frequencies, meaning that the dissipation do not discriminate between low and high-energy excitations, it affects all many-body states with equal strength, regardless of their energy. This energy-insensitive behavior is typical of dephasing processes, which tends to push the system toward a fully mixed state, similar to an infinite-temperature in the infinite time limit.

#### Appendix D: Step-by-step Quantum Boltzmann Equation

In the QBE described in Sec. III B, given the distribution function  $F(\omega, t)$ , the spectrum  $\mathcal{A}$ , the hybridization function  $\Delta$  and the self-energy  $\Sigma$  are updated until DMFT self-consistency is reached. Only after convergence, the distribution function  $F(\omega, t + h)$  is calculated with the QBE (19), and the new NESS loop starts. Here, we consider the case in which DMFT convergence is reached globally in time rather than for each single timestep. We explain how it works. At the first global DMFT iteration,  $n = 0$ , the system is in equilibrium at the initial temperature  $\beta_i$ . The equilibrium functions  $G_{n=0}(\omega, t = 0)$ ,  $\Delta_{n=0}(\omega, t = 0)$ , and  $\Sigma_{n=0}(\omega, t = 0)$  are determined from the same NESS loop described in the Sec. III B in step 1) - 5). At the first global DMFT iteration ( $n = 0$ ), the excitation bath  $\Gamma$  is set to zero for all the timesteps, and the equilibrium Green's functions are not updated in time:

$$\begin{cases} G_{n=0}(\omega, t) \equiv G_0(\omega), & \forall t \\ \Delta_{n=0}(\omega, t) \equiv \Delta_0(\omega), & \forall t \\ \Sigma_{n=0}(\omega, t) \equiv \Sigma_0(\omega), & \forall t \end{cases}$$

Starting from these functions, several global DMFT iterations  $n$ , each of which goes from  $t = 0$  to  $t = t_{\max}$ , are performed until global DMFT convergence is reached. Each full time propagation  $t \in [0, t_{\max}]$  is identified by the index  $n$  ( $n \geq 1$ ). They all start from the same initial condition at  $t = 0$ :

$$\begin{cases} G_n(\omega, t = 0) = G_0(\omega), & \forall n \geq 1 \\ \Delta_n(\omega, t = 0) = \Delta_0(\omega), & \forall n \geq 1 \\ \Sigma_n(\omega, t = 0) = \Sigma_0(\omega), & \forall n \geq 1 \end{cases}$$

Given this initial condition, the DMFT loop for  $t \in [0, t_{\max}]$ , for each full time propagation  $n \geq 1$ , looks like:

1. Update the retarded Green's function:

$$G_n^R(\omega, t) = [\omega + i0^+ - H_{\text{loc},n}(t) - \Delta_n^R(\omega, t) - \Sigma_{\text{int},n}^R(\omega, t)]^{-1}, \quad \forall n \geq 1 \quad (\text{D1})$$

and determine  $\mathcal{A}_n(\omega, t) = -\frac{1}{\pi} \Im G_n^R(\omega + i0, t)$ . We recall that in our case (half-filling) it is always  $H_{\text{loc},n}(t) = 0$ .

2. Determine the lesser Green's function from the given distribution function,

$$G_n^<(\omega, t) = 2\pi i F_n(\omega, t) \mathcal{A}_n(\omega, t), \quad \forall n \geq 1 \quad (\text{D2})$$

3. Use the self-consistency Eq. (9) to fix the hybridization function of the effective steady state impurity model:

$$\begin{cases} \Delta_1^{R,<}(\omega, t) = t_h^2 G_0^{R,<}(\omega, t = 0), & \text{for } n = 1 \\ \Delta_n^{R,<}(\omega, t) = t_h^2 G_{n-1}^{R,<}(\omega, t) + \Gamma_n(\omega, t), & \forall n > 1 \end{cases} \quad (\text{D3})$$

We notice that, for  $n = 1$ ,  $\Delta_1$  is proportional to  $G_0$  for each time-step  $t$ , i.e., the impurity sees a self-consistent bath that is fixed at the initial temperature  $T_i$  during the whole time propagation. Starting from  $n > 1$ , for each timestep  $t$ , the impurity sees a bath which depends on the Green's function at the previous DMFT iteration  $n - 1$ . The self-energy  $\Gamma_n$  that mimics photoexcitation is turned on only for global DMFT  $n > 0$ , since at the very first iteration,  $n = 0$ , the system is kept in the initial equilibrium state for all the times.

4. Solve the impurity model. With IPT as an impurity solver, we first determine  $\mathcal{G}_n(\omega)$  from  $\Delta_n(\omega)$ ,

$$\begin{aligned} \mathcal{G}_n^R(\omega, t) &= [\omega + i0^+ - H_{\text{loc},n}(t) - \Delta_n^R(\omega, t)]^{-1}, \quad \forall n \geq 1 \\ \mathcal{G}_n^<(\omega, t) &= \mathcal{G}_n^R(\omega, t) \Delta_n^<(\omega, t) \mathcal{G}_n^A(\omega, t), \quad \forall n \geq 1 \end{aligned} \quad (\text{D4})$$

then transform to real time, evaluate Eq. (14), and transform back to frequency space to obtain  $\Sigma_{U,n}^{R,<}(\omega)$ .

5. In the time-translational invariant case (NESS loop), the purely dissipative part of the self-energy, Eq. (15), becomes

$$\Sigma_{\gamma,\sigma,n}^{R,<}(\omega, t) = \gamma_n(t) \frac{1}{2\pi} \int d\omega' G_n^{R,<}(\omega', t) \quad (\text{D5})$$

At the first global DMFT iteration,  $n = 0$ ,  $\gamma_{n=0}(t) = 0, \forall t$  since the system is kept in equilibrium at the initial temperature; for  $n > 0$ ,  $\gamma_n(t) : 0 \rightarrow \gamma_f$  at  $t = 0^+$ .

6. Set  $\Sigma_{\text{int},n}(\omega, t) = \Sigma_{U,n}(\omega, t) + \Sigma_{\gamma,\sigma,n}(\omega, t)$ .

7. Update  $F_n$  by means of QBE Eq. (19):

$$\partial_t F_n(\omega, t) = I[F_n(\omega, t), \cdot] \quad (\text{D6})$$

Perform the steps 1)- 6) for the next time  $t + h$  till  $t_{\max}$  is reached. Once  $t_{\max}$  is reached for the iteration  $n$ , the new iteration  $n + 1$  starts. Convergence is reached when, for

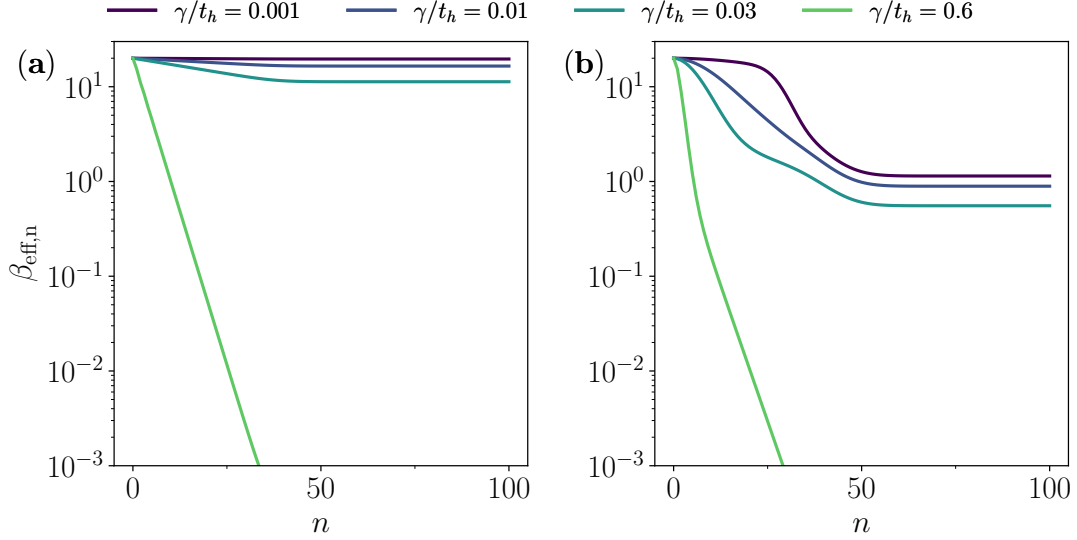


Figure 8. Emergence of Infinite Temperature Thermalization - Evolution of the steady-state effective temperature in the step-by-step DMFT approach, solved with QBE, as a function of the DMFT iteration  $n$  for different values of dephasing  $\gamma/t_h = 0.001, 0.01, 0.03, 0.6$ . The Hubbard interaction is  $U/t_h = 0$  in panel (a) and  $U/t_h = 2$  in panel (b). In both panels, the photo-excitation amplitude is fixed at  $\Gamma/t_h = 1$  and the effective temperature is taken at  $t = 20$ .

each time  $t$ , the functions are not updated significantly from one iteration to the other. We require

$$\sum_{\omega,t} |G_n(\omega, t) - G_{n-1}(\omega, t)| < 10^{-6} \quad (\text{D7})$$

The total energy of the system at iteration  $n$  is

$$E_n(t) = \frac{1}{2\pi} \int d\omega \{ -2i[\Delta_n(\omega, t)G_n(\omega, t)]^< \} \\ \frac{1}{2\pi} \int d\omega \{ -i[\Sigma_{U,n}(\omega, t)G_n(\omega, t)]^< \} \quad (\text{D8})$$

### Appendix E: Excitation protocol

In order to simulate a photo-doping excitation, the system is shortly coupled with a fermionic bath with density of states

$$\mathcal{A}_{\text{bath}}(\omega) = \mathcal{A}_b(\omega - \omega_0) + \mathcal{A}_b(\omega + \omega_0) \quad (\text{E1})$$

consisting of two smooth bands with bandwidth  $W_{\text{bath}} = 4$  centered around the energies  $\omega_0 = \pm 2.5$  [50]. We choose

$$\mathcal{A}_b(\omega) = \frac{1}{\pi} \cos^2(\pi\omega/W_{\text{bath}}) \quad (\text{E2})$$

in the interval  $[\omega_0 - W_{\text{bath}}/2, \omega_0 + W_{\text{bath}}/2]$ . The occupied and unoccupied density of states have spectral shapes given by  $\mathcal{A}_{\text{bath}}^<(\omega) = \mathcal{A}(\omega - \omega_0)$  and  $\mathcal{A}_{\text{bath}}^>(\omega) = \mathcal{A}(\omega + \omega_0)$ , respectively. During the whole time-evolution of the system, the bath occupation  $f_{\text{bath}}(\omega) = f_{-\beta_{\text{bath}}}(\omega)$  is taken to be fixed at negative temperature Fermi-Dirac

distribution (population inversion). In this way, the coupling of the system with the bath mimics photo-excitation. In particular,  $\beta_i$  corresponds to the initial (inverse) temperature of the system (in our calculations,  $\beta_{\text{bath}} \equiv \frac{1}{T_{\text{bath}}} = 20$ ).

This fermionic bath adds a local contribution to the electronic self-energy  $\Sigma$  in Eq. (20), given by

$$\Gamma^{<(>)}(\omega, t) = (-)2\pi i V^2(t) \mathcal{A}_{\text{bath}}^{<(>)}(\omega) \quad (\text{E3})$$

$$\Gamma^R(\omega, t) = -i\pi V^2(t) \mathcal{A}_{\text{bath}}(\omega) \quad (\text{E4})$$

with time-dependent profile

$$V(t) = \Gamma \sin^2(\pi t/T_0) \theta(t) \theta(T_0 - t), \quad (\text{E5})$$

where  $T_0 = 1$  (the pulse duration) in units of hopping times and  $\Gamma$  is the amplitude of the coupling between the system and the bath. In terms of the two times  $(t, t')$  on the Keldysh contour  $\mathcal{C}$ , the bath reads

$$\Gamma(t, t') = V(t) G_{\text{bath}}(t, t') V(t')^*, \quad (\text{E6})$$

where the bath Green's function  $G_{\text{bath}}(t, t')$  is defined as

$$G_{\text{bath}}^R(t, t') = -i\theta(t - t') \int d\omega e^{-i\omega(t-t')} \mathcal{A}_{\text{bath}}(\omega), \quad (\text{E7})$$

$$G_{\text{bath}}^<(t, t') = i \int d\omega e^{-i\omega(t-t')} f_{\text{bath}}(\omega) \mathcal{A}_{\text{bath}}(\omega) \quad (\text{E8})$$

### Appendix F: Emergence of Infinite Temperature Thermalization: steady-state properties.

In this section, we present additional results illustrating the emergence of the infinite-temperature state. As

discussed in Sec. VI, the dynamics observed within the DMFT self-consistency loop deviate from those of purely unitary evolution: the effective temperature does not return to its initial value. Instead, the system evolves toward a prethermal steady state at long times, signaling the onset of thermalization driven by dissipation.

In Fig. 8, we show the inverse temperature  $\beta_{\text{eff},n}$  as a function of the step-by-step DMFT iteration  $n$ , for different values of the dissipation strength  $\gamma$ . For large  $n$ , the effective temperature becomes constant as a function of  $n$ . This means that the step-by-step solution has converged to the full-DMFT one. As the dissipation strength

increases, the final constant value of the effective temperature increases, since the system gets closer to the infinite temperature limit. (For  $\gamma = 0.6$  we don't see the plateau only because it happens for  $\beta \approx 10^{-4}$  for  $U = 0$ , and  $\beta \approx 10^{-5}$  for  $U = 2$ ). The way the effective temperature approaches this plateau depends on the value of the Hubbard interaction  $U$  (and  $\gamma$ ). For  $U = 0$  (Fig 8 (a)), the decay is exponential with  $n$  for all  $\gamma$ . For  $U = 2$  (Fig 8 (b)), it shows a double-exponential decay for  $\gamma = 0.6$ . For lower values of  $\gamma$ , the system spends more and more time at equilibrium at the initial temperature  $\beta_i = 20$ , before relaxing to the final state with a non-trivial dynamics.

- 
- [1] R. Fazio, J. Keeling, L. Mazza, and M. Schirò, *Many-body open quantum systems* (2025), [arXiv:2409.10300 \[quant-ph\]](#).
  - [2] L. M. Sieberer, M. Buchhold, J. Marino, and S. Diehl, Universality in driven open quantum matter, *Rev. Mod. Phys.* **97**, 025004 (2025).
  - [3] H. P. Breuer and F. Petruccione, *The Theory of Open Quantum Systems*, 1st ed., Vol. 9780199213 (OUP Oxford, 2007).
  - [4] M. Esposito and P. Gaspard, Exactly solvable model of quantum diffusion, *Journal of Statistical Physics* **121**, 463 (2005).
  - [5] M. Esposito and P. Gaspard, Emergence of diffusion in finite quantum systems, *Phys. Rev. B* **71**, 214302 (2005).
  - [6] M. Žnidarič, Exact solution for a diffusive nonequilibrium steady state of an open quantum chain, *Journal of Statistical Mechanics: Theory and Experiment* **2010**, L05002 (2010).
  - [7] V. Eisler, Crossover between ballistic and diffusive transport: the quantum exclusion process, *Journal of Statistical Mechanics: Theory and Experiment* **2011**, P06007 (2011).
  - [8] M. Žnidarič and M. Horvat, Transport in a disordered tight-binding chain with dephasing, *The European Physical Journal B* **86**, 67 (2013).
  - [9] Z. Cai and T. Barthel, Algebraic versus exponential decoherence in dissipative many-particle systems, *Phys. Rev. Lett.* **111**, 150403 (2013).
  - [10] M. V. Medvedyeva, F. H. L. Essler, and T. c. v. Prosen, Exact bethe ansatz spectrum of a tight-binding chain with dephasing noise, *Phys. Rev. Lett.* **117**, 137202 (2016).
  - [11] X. Turkeshi and M. Schirò, Diffusion and thermalization in a boundary-driven dephasing model, *Phys. Rev. B* **104**, 144301 (2021).
  - [12] V. Alba and F. Carollo, Spreading of correlations in Markovian open quantum systems, *Phys. Rev. B* **103**, L020302 (2021).
  - [13] T. Jin, J. S. Ferreira, M. Filippone, and T. Giamarchi, Exact description of quantum stochastic models as quantum resistors, *Phys. Rev. Res.* **4**, 013109 (2022).
  - [14] D. Wellnitz, G. Preisser, V. Alba, J. Dubail, and J. Schachenmayer, Rise and fall, and slow rise again, of operator entanglement under dephasing, *Phys. Rev. Lett.* **129**, 170401 (2022).
  - [15] A. G. Catalano, F. Mattiotti, J. Dubail, D. Hagenmüller, T. Prosen, F. Franchini, and G. Pupillo, Anomalous diffusion in the long-range haken-strobl-reineker model, *Phys. Rev. Lett.* **131**, 053401 (2023).
  - [16] A. Marché, G. Morettini, L. Mazza, L. Gotta, and L. Capizzi, Exceptional stationary state in a dephasing many-body open quantum system, *Phys. Rev. Lett.* **135**, 020406 (2025).
  - [17] F. Gerbier and Y. Castin, Heating rates for an atom in a far-detuned optical lattice, *Phys. Rev. A* **82**, 013615 (2010).
  - [18] H. Pichler, A. J. Daley, and P. Zoller, Nonequilibrium dynamics of bosonic atoms in optical lattices: Decoherence of many-body states due to spontaneous emission, *Phys. Rev. A* **82**, 063605 (2010).
  - [19] S. Sarkar, S. Langer, J. Schachenmayer, and A. J. Daley, Light scattering and dissipative dynamics of many fermionic atoms in an optical lattice, *Phys. Rev. A* **90**, 023618 (2014).
  - [20] Y. Yanay and E. J. Mueller, Heating from continuous number density measurements in optical lattices, *Phys. Rev. A* **90**, 023611 (2014).
  - [21] D. Poletti, J.-S. Bernier, A. Georges, and C. Kollath, Interaction-induced impeding of decoherence and anomalous diffusion, *Phys. Rev. Lett.* **109**, 045302 (2012).
  - [22] D. Poletti, P. Barmettler, A. Georges, and C. Kollath, Emergence of glasslike dynamics for dissipative and strongly interacting bosons, *Phys. Rev. Lett.* **111**, 195301 (2013).
  - [23] R. Bouganne, M. Bosch Aguilera, A. Ghermaoui, J. Beugnon, and F. Gerbier, Anomalous decay of coherence in a dissipative many-body system, *Nature Physics* **16**, 21 (2020).
  - [24] J.-S. Bernier, R. Tan, L. Bonnes, C. Guo, D. Poletti, and C. Kollath, Light-cone and diffusive propagation of correlations in a many-body dissipative system, *Phys. Rev. Lett.* **120**, 020401 (2018).
  - [25] R. Vatré, R. Bouganne, M. B. Aguilera, A. Ghermaoui, J. Beugnon, R. Lopes, and F. Gerbier, Dynamics of spatial phase coherence in a dissipative Bose-Hubbard atomic system, *Comptes Rendus. Physique* **24**, 263 (2023).
  - [26] M. Buchhold and S. Diehl, Nonequilibrium universality in the heating dynamics of interacting luttinger liquids, *Phys. Rev. A* **92**, 013603 (2015).
  - [27] J.-S. Bernier, R. Tan, C. Guo, C. Kollath, and D. Poletti, Melting of the critical behavior of a tomonaga-luttinger

- liquid under dephasing, *Phys. Rev. B* **102**, 115156 (2020).
- [28] A. Bácsi, C. P. Moca, G. Zaránd, and B. Dóra, Vaporization dynamics of a dissipative quantum liquid, *Phys. Rev. Lett.* **125**, 266803 (2020).
  - [29] J. Tindall, B. Buča, J. R. Coulthard, and D. Jaksch, Heating-induced long-range  $\eta$  pairing in the hubbard model, *Phys. Rev. Lett.* **123**, 030603 (2019).
  - [30] J.-S. Bernier, D. Poletti, and C. Kollath, Dissipative quantum dynamics of fermions in optical lattices: A slave-spin approach, *Phys. Rev. B* **90**, 205125 (2014).
  - [31] A. J. Daley, I. Bloch, C. Kokail, S. Flannigan, N. Pearson, M. Troyer, and P. Zoller, Practical quantum advantage in quantum simulation, *Nature* **607**, 667 (2022).
  - [32] M. Xu, L. H. Kendrick, A. Kale, Y. Gang, C. Feng, S. Zhang, A. W. Young, M. Lebrat, and M. Greiner, A neutral-atom hubbard quantum simulator in the cryogenic regime, *Nature* **642**, 909 (2025).
  - [33] T. Chalopin, P. Bojović, S. Wang, T. Franz, A. Sinha, Z. Wang, D. Bourgund, J. Obermeyer, F. Grusdt, A. Bohrdt, L. Pollet, A. Wietek, A. Georges, T. Hilker, and I. Bloch, Probing the magnetic origin of the pseudogap using a fermi-hubbard quantum simulator (2024), [arXiv:2412.17801 \[cond-mat.str-el\]](https://arxiv.org/abs/2412.17801).
  - [34] V. Korolev, T. Lettau, V. Krishna, A. Croy, M. Zuerch, C. Spielmann, M. Waechtler, U. Peschel, S. Graefe, G. Soavi, and D. Kartashov, Unveiling the role of electron-phonon scattering in dephasing high-order harmonics in solids (2024), [arXiv:2401.12929 \[physics.optics\]](https://arxiv.org/abs/2401.12929).
  - [35] A. Georges, G. Kotliar, W. Krauth, and M. J. Rozenberg, Dynamical mean-field theory of strongly correlated fermion systems and the limit of infinite dimensions, *Rev. Mod. Phys.* **68**, 13 (1996).
  - [36] H. Aoki, N. Tsuji, M. Eckstein, M. Kollar, T. Oka, and P. Werner, Nonequilibrium dynamical mean-field theory and its applications, *Rev. Mod. Phys.* **86**, 779 (2014).
  - [37] O. Scarlatella, A. A. Clerk, R. Fazio, and M. Schiró, Dynamical mean-field theory for markovian open quantum many-body systems, *Physical Review X* **11**, 10.1103/physrevx.11.031018 (2021).
  - [38] M. Vanhoecke and M. Schiró, Diagrammatic monte carlo for dissipative quantum impurity models, *Phys. Rev. B* **109**, 125125 (2024).
  - [39] M. Vanhoecke and M. Schiró, Kondo-zeno crossover in the dynamics of a monitored quantum dot, *Nature Communications* **16**, 6155 (2025).
  - [40] A. Picano, G. Biroli, and M. Schiró, Quantum thermalization via travelling waves, *Phys. Rev. Lett.* **134**, 116503 (2025).
  - [41] A. Kamenev, *Field Theory of Non-Equilibrium Systems* (Cambridge University Press, 2011).
  - [42] L. M. Sieberer, M. Buchhold, and S. Diehl, Keldysh field theory for driven open quantum systems, *Reports on Progress in Physics* **79**, 096001 (2016).
  - [43] G. Stefanucci, Kadanoff-baym equations for interacting systems with dissipative lindbladian dynamics, *Phys. Rev. Lett.* **133**, 066901 (2024).
  - [44] C. Stahl, N. Dasari, J. Li, A. Picano, P. Werner, and M. Eckstein, Memory truncated kadanoff-baym equations, *Phys. Rev. B* **105**, 115146 (2022).
  - [45] A. Picano, J. Li, and M. Eckstein, Quantum boltzmann equation for strongly correlated electrons, *Phys. Rev. B* **104**, 085108 (2021).
  - [46] A. Mitra and T. Giamarchi, Mode-coupling-induced dissipative and thermal effects at long times after a quantum quench, *Phys. Rev. Lett.* **107**, 150602 (2011).
  - [47] M. Schiró and A. Mitra, Transient orthogonality catastrophe in a time-dependent nonequilibrium environment, *Phys. Rev. Lett.* **112**, 246401 (2014).
  - [48] A. Larzul and M. Schiró, Quenches and (pre)thermalization in a mixed sachdev-ye-kitaev model, *Phys. Rev. B* **105**, 045105 (2022).
  - [49] T. Jin, J. a. S. Ferreira, M. Filippone, and T. Giamarchi, Exact description of quantum stochastic models as quantum resistors, *Phys. Rev. Research* **4**, 013109 (2022).
  - [50] A. Picano, F. Grandi, and M. Eckstein, Inhomogeneous disordering at a photoinduced charge density wave transition, *Phys. Rev. B* **107**, 245112 (2023).